
Pre-trained Encoder Inference: Revealing Upstream Encoders In Downstream Machine Learning Services

Shaopeng Fu¹ Xuexue Sun² Ke Qing³ Tianhang Zheng⁴ Di Wang¹

¹King Abdullah University of Science and Technology ²HitoX

³University of Science and Technology of China ⁴Zhejiang University

shaopeng.fu@kaust.edu.sa, snows.yanzhi@gmail.com

qingkeld@mail.ustc.edu.cn, zthzheng@gmail.com, di.wang@kaust.edu.sa

Abstract

Pre-trained encoders available online have been widely adopted to build downstream machine learning (ML) services, but various attacks against these encoders also pose security and privacy threats toward such a downstream ML service paradigm. We unveil a new vulnerability: the *Pre-trained Encoder Inference (PEI)* attack, which can extract sensitive encoder information from a targeted downstream ML service that can then be used to promote other ML attacks against the targeted service. By only providing API accesses to a targeted downstream service and a set of candidate encoders, the PEI attack can successfully infer which encoder is secretly used by the targeted service based on candidate ones. Compared with existing encoder attacks, which mainly target encoders on the upstream side, the PEI attack can compromise encoders even after they have been deployed and hidden in downstream ML services, which makes it a more realistic threat. We empirically verify the effectiveness of the PEI attack on *vision* encoders. we first conduct PEI attacks against two downstream services (*i.e.*, image classification and multimodal generation), and then show how PEI attacks can facilitate other ML attacks (*i.e.*, model stealing attacks *vs.* image classification models and adversarial attacks *vs.* multimodal generative models). Our results call for new security and privacy considerations when deploying encoders in downstream services. The code is available at <https://github.com/fshp971/encoder-inference>.

1 Introduction

Recent advances of self-supervised learning (SSL) [15, 54, 28, 70, 55, 10] and the availability of large amounts of public unlabeled data have enabled the pre-training of powerful representation encoders. These pre-trained encoders are usually first built by upstream suppliers who control sufficient computational resources and then delivered through online model repositories (*e.g.*, Hugging Face) or *Encoder-as-a-Service (EaaS)* to downstream suppliers to help them quickly build their own machine learning (ML) services. Specifically, one can simply use an encoder to encode downstream training data to informative embeddings and train downstream models upon them with relatively little cost. These downstream models are eventually provided as service APIs to end users.

Despite the success of this *upstream pre-training, downstream quick-building* paradigm, many attacks also emerge to threaten pre-trained encoders and further compromise the security and privacy of downstream ML services. These encoder attacks typically begin by compromising encoders in the pre-training stage via poisoning [6] or backdooring [35]. Then, when an attacked encoder is deployed in a downstream ML service, it will enable the adversary to manipulate the behavior of the downstream model [42, 60] or leak private information of downstream data [67, 21]. To mitigate these attacks,

efforts have been made during the encoder pre-training stage to enhance the robustness of encoders against adversaries [49, 61] or perform source tracing when an attack has occurred [46, 13, 18].

This paper focuses on a more challenging setting where a *clean* pre-trained encoder (*i.e.*, not affected by encoder attacks) has already been deployed into the targeted service and the adversary only has API access to this service. Under this setting, previous poisoning/backdooring-based encoder attacks, which need to access and modify the pipeline of building downstream ML services, all become invalid. In this sense, both encoders and downstream ML services seem to be much safer. **Unfortunately, we unveil a new class of encoder privacy attacks named *Pre-trained Encoder Inference (PEI)* attack, showing that downstream services and their encoders are still vulnerable to adversaries from the downstream side even under such a “safer setting”.** As shown in Figure 1, given a targeted downstream ML service, the goal of the new PEI attack is to infer what pre-trained encoder is secretly used by the downstream model. Once the hidden encoder is revealed, the adversary can then exploit public APIs of the hidden encoder to facilitate other ML attacks against the targeted downstream service such as model stealing attacks or adversarial attacks more effectively.

To launch a PEI attack against a targeted downstream ML service that is built upon a hidden encoder f^* , we assume that the adversary has API accesses to the targeted service and a set E consisting of several candidate pre-trained encoders from online model repositories or EaaS. The goal of the PEI adversary is to infer: (1) whether $f^* \in E$ and (2) which candidate from E is the hidden f^* . Realizing the PEI attack relies on the observation that **for any certain encoder and a pre-defined embedding, there exist samples that look different from each other but enjoy embeddings similar to that pre-defined one only under such a certain encoder**. Under this observation, to infer whether a given candidate encoder is used by the targeted service, we propose to first synthesize a series of *PEI attack samples* via minimizing the difference of their embeddings and the pre-defined embedding under this candidate encoder. Then, we evaluate whether these synthesized PEI attack samples can make the targeted service produce a specified behavior determined by that pre-defined embedding. Notably, our framework makes no assumptions about downstream tasks, and thus can work in a downstream-task agnostic manner as long as the PEI attack samples are synthesized.

We conduct experiments on *vision* encoders used in two downstream tasks: *image classification* and *multimodal generation* (*i.e.*, the LLaVA model [40, 41]), to demonstrate the effectiveness of the proposed PEI attack. For each targeted downstream service, **we first conduct the PEI attack against the hidden encoder** and demonstrate that the PEI attack successfully reveals hidden encoders in most targeted services, with a cost as low as an estimated \$100 per candidate encoder. Moreover, our attack never makes false-positive predictions, even when the correct hidden encoder is not in the candidate set. Then, **we study how the hidden encoder revealed by the PEI attack can facilitate other ML attacks against the targeted service**. For the image classification service, we show that the PEI attack can improve model stealing attacks [63] in both *accuracy* and *fidelity* by $2 \sim 20$ times. For the multimodal generative service, we analyze how the revealed encoder can assist in synthesizing adversarial images to stealthily spread false medical/health information through the targeted service.

Due to space limitations, discussions on related works are included in Appendix A.

2 Preliminaries

2.1 Pre-trained encoders

A pre-trained encoder is a function $f : \mathcal{X} \rightarrow \mathcal{E}$ that can encode any sample $x \in \mathcal{X}$ to an informative embedding vector $f(x)$. This powerful encoding ability can be used to facilitate building downstream

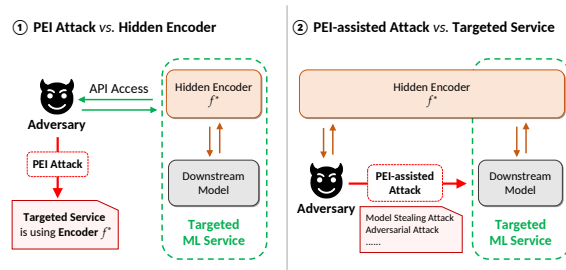


Figure 1: Illustration of how the PEI attack can threaten downstream ML services. **Step 1:** Using the PEI attack to reveal the encoder hidden in the targeted downstream service. **Step 2:** Exploiting the revealed encoder to conduct other ML attacks, *e.g.*, model stealing and adversarial attacks, against the original targeted service.

ML services. Concretely, suppose there is a downstream task-specific dataset $D = \{(x_i, y_i)\}_{i=1}^{|D|}$, where $x_i \in \mathcal{X}$ is the i -th downstream sample and $y_i \in \mathcal{Y}$ is its label. To build an ML service to handle the downstream task, the service supplier will encode each downstream sample x_i to $f(x_i)$, and train a downstream model h_θ on these encoded embeddings as follows,

$$\min_{\theta} \frac{1}{|D|} \sum_{(x_i, y_i) \in D} \ell(h_\theta(f(x_i)), y_i),$$

where $\ell : \mathcal{Y} \times \mathcal{Y} \rightarrow \mathbb{R}^+$ is a downstream task-dependent loss function and θ is the downstream model parameter. After that, the downstream ML service will be made online and provide API access to end users, where the API is powered by the composite function $h_\theta(f(\cdot)) : \mathcal{X} \rightarrow \mathcal{Y}$. Whenever a query x comes, the API will return $h_\theta(f(x))$ as the response.

2.2 Threat model

The threat model of the PEI attack consists of two parties: (1) the *targeted downstream ML service* $g : \mathcal{X} \rightarrow \mathcal{Y}$, and (2) the *PEI adversary*.

Targeted downstream ML service g . The targeted service can be seen as a composite function $g(\cdot) := h_\theta(f^*(\cdot))$, where f^* is the encoder secretly used in the downstream service and h_θ is the downstream model trained following the pipeline described in Section 2.1. It is notable that this targeted service g can only be accessed through APIs: for any query sample x from end-users, the service will only return $g(x)$ as the response. Other operations are not allowed.

Adversary’s goal. The goal of a PEI adversary is to reveal the encoder f^* hidden by the targeted service g . Concretely, suppose the adversary holds a set $E = \{f_1, \dots, f_N\}$ consisting of N publicly accessible pre-trained encoders that may from online model repositories or EaaS. The adversary aims to: (1) determine whether the hidden f^* comes from the candidates set E , and (2) if it is determined that $f^* \in E$, infer which candidate $f_i \in E$ is the hidden f^* .

Adversary’s capabilities. We assume that the adversary has the following capabilities:

- **API access to the targeted service.** The adversary can query the targeted service g with any sample x and receive $g(x)$ as the return. It is notable that the adversary has no prior knowledge about the downstream model h_θ and the hidden encoder f^* and is not allowed to directly interact with or modify the hidden encoder f^* .
- **API access to candidate encoders.** For each candidate $f_i \in E$, the adversary can query it with any sample x and receive $f_i(x)$ as the return. However, the adversary could not access the model parameter of f_i . We argue that the size of the candidate set does not need be too large, as real-world applications usually tend to use EaaS/pre-trained encoders provided by a few reputable tech companies (e.g., OpenAI, Hugging Face, Microsoft, and Google).

3 Designing Pre-trained Encoder Inference (PEI) attack

3.1 Intuition of the design

The high-level design of the PEI attack is motivated by the observation that for a certain encoder and a pre-defined embedding, samples always exist that look different but enjoy embeddings similar to that pre-defined one only under this encoder. Further, when the encoder is changed, the embeddings of these samples will again become different. We named such kind of samples as *PEI attack samples* corresponding to the certain encoder, and they will be the key ingredient of our attack framework.

The idea is that for a targeted downstream service that is built upon this certain encoder, the corresponding PEI attack samples are very likely to make the downstream model produce a specific behavior determined by the pre-defined embedding. Besides, when the hidden encoder behind the targeted service is not the aforementioned certain encoder, such a specific behavior is less likely to be produced by the downstream model. Thus, the adversary can exploit this behavior discrepancy to perform the PEI attack against downstream ML services.

Algorithm 1 PEI Attack Framework

Input: Targeted downstream ML service g , candidate encoders f_1, \dots, f_N , objective samples $x_1^{(obj)}, \dots, x_{M_1}^{(obj)}$, Downstream service behavior similarity function ℓ_{sim} .

Output: Encoder \hat{f}^* inferred via the PEI attack.

- 1: **for** i in $1, \dots, N$ **do** ▷ PEI Attack Samples Synthesis Stage Started
- 2: Synthesize $\{x_{i,j,k}^{(atk)}\}_{k=1}^{M_2}$ via first randomly initializing them and then minimizing Eq. (1) based on f_i , $x_j^{(obj)}$, and a zeroth-order optimizer.
- 3: **end for**
- 4: **for** i in $1, \dots, N$ **do** ▷ Hidden Encoder Inference Stage Started
- 5: Calculate the PEI score ζ_i following Eq. (2) based on g , f_i , $\{x_j^{(obj)}\}_{j=1}^{M_1}$ and $\{x_{i,j,k}^{(atk)}\}_{j=1,k=1}^{M_1,M_2}$.
- 6: **end for**
- 7: Calculate z_1, \dots, z_N following Eq. (3).
- 8: $I \leftarrow \{i : z_i > 1.7\}$
- 9: **if** $|I| = 1$ **then**
- 10: **return** $\hat{f}^* \leftarrow f_{i^*}$ ▷ i^* is the only element in set I .
- 11: **end if**
- 12: **return** $\hat{f}^* \leftarrow \emptyset$

3.2 General attack framework

As explained before, finding PEI attack samples for different (candidate) encoders is a vital step in the PEI attack. In our attack framework, we propose to *synthesize* such attack samples for each encoder independently. This results in a two-stage PEI attack design: (1) **PEI attack samples synthesis stage**, and (2) **hidden encoder inference stage**. The overall implementation of the attack is presented as Algorithm 1. We now introduce the two stages in detail.

PEI attack samples synthesis stage. In this stage, the adversary first collects M_1 samples $\{x_j^{(obj)}\}_{j=1}^{M_1}$ named *objective samples* from public data domains. Then, for each encoder-sample pair $(f_i, x_j^{(obj)})$ where $f_i \in E$ is the i -th candidate encoder and $x_j^{(obj)}$ is the j -th objective sample, the adversary synthesizes a set of M_2 PEI attack samples $\{x_{i,j,k}^{(atk)}\}_{k=1}^{M_2}$. Each $x_{i,j,k}^{(atk)}$ for the pair $(f_i, x_j^{(obj)})$ is first randomly initialized and then obtained via minimizing the below squared loss $\mathcal{L}_{i,j}$,

$$\mathcal{L}_{i,j}(x_{i,j,k}^{(atk)}) = \|f_i(x_{i,j,k}^{(atk)}) - f_i(x_j^{(obj)})\|_2^2. \quad (1)$$

Intuitively, Eq. (1) aims to make the embeddings of the PEI attack sample $x_{i,j,k}^{(atk)}$ and the objective sample $x_j^{(obj)}$ under the candidate encoder f_i similar to each other in l_2 -distance. To minimize Eq. (1), a naive solution is to use gradient descent methods. However, since our threat model only assumes API access to the candidate encoder f_i , the adversary cannot calculate first-order gradients of Eq. (1), which makes simple gradient descent methods be invalid.

Hidden encoder inference stage. For the encoder f^* hidden in the targeted downstream ML service $g(\cdot) := h_\theta(f^*(\cdot))$, the adversary exploits synthesized PEI attack samples to infer: (1) whether $f^* \in E$ or not and (2) if so, which $f_i \in E$ is f^* . We argue that these two goals can be solved simultaneously. Concretely, we propose to first calculate N PEI scores ζ_1, \dots, ζ_N for the N candidates, where each ζ_i is calculated based on objective samples $x_1^{(obj)}, \dots, x_{M_1}^{(obj)}$ and PEI attack samples $\{x_{i,j,k}^{(atk)} : j \leq M_1, k \leq M_2\}$ of the candidate $f_i \in E$ as follows,

$$\zeta_i = \frac{1}{M_1 M_2} \sum_{j=1}^{M_1} \sum_{k=1}^{M_2} \ell_{sim} \left(g(x_{i,j,k}^{(atk)}), g(x_j^{(obj)}) \right), \quad (2)$$

where $\ell_{sim} : \mathcal{Y} \times \mathcal{Y} \rightarrow \mathbb{R}^+$ is a task-dependent function that measures the similarity of behaviors produced by the targeted service g . A larger output $\ell_{sim}(\cdot, \cdot)$ means the corresponding two inputs are more similar to each other. Among the N PEI scores, if there happens to be a single score, denoted as ζ_{i^*} , that is significantly higher than others, one can thus conclude that $f^* \in E$ and $f^* = f_{i^*}$, otherwise conclude $f^* \notin E$. After that, the two PEI attack goals have been accomplished.

Algorithm 2 Black-box PEI Attack Sample Synthesis (via Solving Eq. (1)) for Vision Encoder

Input: Candidate vision encoder f_i , objective image sample $x_j^{(obj)}$, random sampling number S , perturbation radius $\epsilon > 0$, training iteration T , learning rate η .

Output: Synthesized PEI attack sample $x_{i,j,k}^{(atk)}$.

- 1: Initialize $x_{i,j,k}^{(atk)}$ with uniform distribution $\mathcal{U}[0, 1]^{\dim(\mathcal{X})}$.
- 2: Denote $\mathcal{L}_{i,j}(x) := \|f_i(x) - f_i(x_j^{(obj)})\|_2^2$.
- 3: **for** t in $1, \dots, T$ **do**
- 4: Draw S directions $\mu_1, \dots, \mu_S \sim \mathbb{S}^{\dim(\mathcal{X})-1}$.
- 5: Estimate gradient $\nabla_x \mathcal{L}_{i,j}(x_{i,j,k}^{(atk)})$ following Eq. (5) based on ϵ and μ_1, \dots, μ_S .
- 6: Update $x_{i,j,k}^{(atk)}$ via gradient normalization: $x_{i,j,k}^{(atk)} \leftarrow x_{i,j,k}^{(atk)} - \frac{\eta \cdot \nabla_x \mathcal{L}_{i,j}(x_{i,j,k}^{(atk)})}{\|\nabla_x \mathcal{L}_{i,j}(x_{i,j,k}^{(atk)})\|_\infty}$.
- 7: Clip $x_{i,j,k}^{(atk)}$ into the range $[0, 1]^{\dim(\mathcal{X})}$.
- 8: **end for**
- 9: **return** $x_{i,j,k}^{(atk)}$

Based on the above analysis, the remaining task to complete the PEI attack is to find a way to assess whether a given PEI score is truly significantly higher than others. Here we adopt a simple yet efficient *one-tailed z-test* to realize our goal. Specifically, for each PEI score ζ_i , if the candidate encoder f_i is not the hidden one f^* , then the score ζ_i would be relatively low. As a result, we can check whether ζ_i is significantly high by testing the following null hypothesis,

$H_0^{(i)}$: The PEI score ζ_i is **NOT** calculated based on PEI attack samples for the hidden encoder f^* .

If $H_0^{(i)}$ is rejected, then ζ_i will be determined to be significantly high and f_i will be inferred as the hidden f^* . We then construct the following statistic *z-score* to evaluate the null hypothesis,

$$z_i = (\zeta_i - \mathbb{E}[\zeta_{i'}]_{i'=1}^N) / (\text{SD}[\zeta_{i'}]_{i'=1}^N), \quad (3)$$

where $\mathbb{E}[\zeta_{i'}]_{i'=1}^N$ and $\text{SD}[\zeta_{i'}]_{i'=1}^N$ are the mean and the sample standard deviation of the N candidate PEI scores ζ_1, \dots, ζ_N . If z_i is above a chosen threshold, then the null hypothesis $H_0^{(i)}$ will be rejected. We further assume that the distribution of PEI scores calculated based on non-hidden encoders' PEI attack samples can be approximated by a normal distribution. In this case, if we chose $z_i > 1.7$ as the rejection criterion, it will lead to a one-sided *p*-value, which is also the false-positive rate, of 4.45%. Since such a *p*-value is smaller than the typical statistical significance level (which is 5%), we thus set the criterion as $z_i > 1.7$, which eventually leads to the following inference attack,

$$\hat{f}^* = \begin{cases} f_{i^*} & (|\{i : z_i > 1.7\}| = 1 \text{ and } z_{i^*} > 1.7) \\ \emptyset & (\text{otherwise}) \end{cases}, \quad (4)$$

where \emptyset means that no candidate is inferred as the hidden encoder f^* by the PEI attack.

Comparison with existing works. We acknowledge that the idea of synthesizing data of similar embeddings has also been adopted by [46] to design encoder watermarks that can be verified in downstream services. However, their method is only a watermarking method, while the PEI is a type of privacy attack against pre-trained encoders. It is also worth noting that [46] is a white-box protection that requires accessing full parameters of pre-trained encoders to inject watermarks, while our PEI attack is a black-box attack that can work as long as black-box accesses to candidate encoders and targeted downstream services are provided.

3.3 PEI attack samples synthesis for vision encoders

Finally, we present how to apply the proposed PEI attack (Algorithm 1) to threaten *vision* encoders deployed in downstream services. The main technical challenge lies in how to solve the PEI attack sample synthesis objective function $\mathcal{L}_{i,j}(x)$ defined in Eq. (1) in a black-box manner. Since when candidate encoders f_1, \dots, f_N are vision encoders, the function $\mathcal{L}_{i,j}(x)$ can be seen as a continuous function for the input image x . Thus, one can leverage zeroth-order gradient estimation techniques to

estimate the gradient of the function $\mathcal{L}_{i,j}(x)$ in a black-box manner and use gradient-based methods to solve Eq. (1). Such techniques are widely adopted to attack black-box vision models [36, 65].

We use the two-point zeroth-order gradient estimation [44, 17] method to solve Eq. (1) for the vision encoder f_i . Specifically, for the objective function $\mathcal{L}_{i,j}(x)$ in Eq. (1), its gradient is estimated as

$$\nabla_x \mathcal{L}_{i,j}(x) \approx \frac{\dim(\mathcal{X})}{S} \sum_{s=1}^S \frac{\mathcal{L}_{i,j}(x + \epsilon \mu_s) - \mathcal{L}_{i,j}(x - \epsilon \mu_s)}{2\epsilon} \mu_s, \quad (5)$$

where S is the estimation random sampling number, $\epsilon > 0$ is the estimation perturbation radius, and $\{\mu_s\}_{s=1}^S$ are i.i.d. random vectors in the same shape of \mathcal{X} drawn from the unit sphere $\mathbb{S}^{\dim(\mathcal{X})-1}$. A larger sampling number S will result in a more accurate gradient estimation but a higher encoder querying budget. We further adopt l_∞ -norm gradient normalization during the optimization to relieve the difficulty of turning learning rate η (as now we can explicitly control the maximum pixel updating values). The overall procedures of solving Eq. (1) for vision encoder are presented as Algorithm 2.

Query budget. We focus on analyzing the black-box query budget of synthesizing PEI attack samples for single candidates. According to Algorithm 1, such a query budget for a single candidate encoder is $\mathcal{O}(M_1 \cdot M_2 \cdot C)$, where $\mathcal{O}(C)$ is the query budget for solving Eq. (1). Then, according to Algorithm 2, solving Eq. (1) for a single vision encoder requires a query budget of $\mathcal{O}(C) = \mathcal{O}(T \cdot 2S)$. All these lead to a query budget for synthesizing PEI attack images of $\mathcal{O}(M_1 \cdot M_2 \cdot T \cdot 2S)$ per candidate encoder. Our experiments in Section 4 and Section 5 show that setting $M_1 = 10$, $M_2 = 5$, $T = 100$, and $S = 100$ is enough to perform an effective PEI attack against vision encoders. This results in an attack cost estimated based on real-world EaaS prices of no more \$100 per candidate encoder.

4 Experiments on image classification services

In this section, we first analyze how the PEI attack can reveal vision encoders in image classification services and then show how revealed encoders can assist model stealing against targeted services.

4.1 Experimental setup

Building downstream services. We adopt three downstream image datasets, which are: **CIFAR-10** [37], **SVHN** [47], and **Food-101** [2]. Six vision encoders from the Hugging Face Model Repository are adopted as candidates in the PEI attack, which are: **ResNet-34 (HF)** [29], **ResNet-50 (HF)**, **MobileNetV3** [32], **ResNet-34 (MS)**, **ResNet-50 (MS)**, and **CLIP ViT-L/14** [54]. The first three encoders were built by Hugging Face, the forth and fifth were built by Microsoft, and the last was built by OpenAI. For each pair of encoder and downstream dataset, we fix the encoder and train a downstream classifier, which is a MLP, based on embeddings of downstream training data obtained from the encoder. See Appendix B.1 for more details about the downstream services building.

PEI attack image synthesis. We randomly select $M_1 = 10$ images from the PASCAL VOC 2012 dataset [20] as the objective samples $\{x_i^{(obj)}\}_{i=1}^{M_1}$. They are collected and presented as Figure 4 in Appendix B.2. For each pair of candidate encoder f_i and objective sample $x_j^{(obj)}$, we follow Algorithm 2 to synthesize $M_2 = 5$ PEI attack images $\{x_{i,j,k}^{(atk)}\}_{k=1}^{M_2}$. Meanwhile, the perturbation radius ϵ is set as 5.0, the sampling number S is set as 100, the training iterations number T is set as 100, and the learning rate is fixed to 0.1. The shape of each synthesized PEI attack image is 64×64 .

PEI score calculation. To calculate the PEI score ζ_i via Eq. (2), the adversary needs to have a task-dependent similarity function ℓ_{sim} . In this section, for classification tasks, we leverage the indicator function $1[\cdot]$ and calculate the PEI score as $\zeta_i = \frac{1}{M_1 M_2} \sum_{j=1}^{M_1} \sum_{k=1}^{M_2} 1[g(x_j^{(obj)}) = g(x_{i,j,k}^{(atk)})]$.

4.2 Results analysis

Classification accuracies of the built 18 image classification services (6 encoders \times 3 downstream datasets) are reported as Table 5 (Appendix B.3). We then study the performance of the PEI attack.

The PEI attack is extremely effective in image classification services. The PEI scores and z -scores of candidate vision encoders in different image classification services are reported in Table 1, showing

Table 1: PEI scores and PEI z -scores of candidate encoders on different downstream image classification services. If a candidate has z -score that is the only one above the threshold, then it is inferred as the encoder hidden in the service. **Blue color** means that the hidden encoder is correctly revealed, while **red color** means that the PEI attack fails.

Dataset	Downstream Task	Encoder	RN34 (HF)	Candidate Encoder	PEI Score (%) / PEI z -Score (Threshold = 1.7)	MobileNetV3	CLIP ViT-L/14	Inferred Encoder
			RN50 (HF)	RN34 (MS)	RN50 (MS)			
CIFAR-10	RN34 (HF)	RN34 (HF)	52.0 / 2.04	2.0 / -0.33	0.0 / -0.43	0.0 / -0.43	0.0 / -0.43	RN34 (HF)
		RN50 (HF)	14.0 / -0.28	50.0 / 2.01	10.0 / -0.53	16.0 / -0.15	10.0 / -0.53	RN50 (HF)
		RN34 (MS)	36.0 / -0.82	40.0 / -0.20	54.0 / 1.94	38.0 / -0.51	42.0 / 0.10	RN34 (MS)
	RN50 (HF)	RN50 (MS)	0.0 / -0.77	22.0 / 0.47	2.0 / -0.65	46.0 / 1.81	2.0 / -0.65	RN50 (MS)
		MobileNetV3	0.0 / -0.41	0.0 / -0.41	0.0 / -0.41	0.0 / -0.41	36.0 / 2.04	MobileNetV3
		CLIP ViT-L/14	20.0 / -0.41	20.0 / -0.41	20.0 / -0.41	20.0 / -0.41	50.0 / 2.04	CLIP ViT-L/14
SVHN	RN34 (HF)	RN34 (HF)	58.0 / 1.98	4.0 / -0.86	14.0 / -0.33	16.0 / -0.23	14.0 / -0.33	RN34 (HF)
		RN50 (HF)	30.0 / -0.28	46.0 / 1.99	30.0 / -0.28	30.0 / -0.28	26.0 / -0.85	RN50 (HF)
		RN34 (MS)	16.0 / -0.40	16.0 / -0.40	36.0 / 1.78	16.0 / -0.40	24.0 / 0.47	RN34 (MS)
	RN50 (HF)	RN50 (MS)	24.0 / 0.70	12.0 / -0.98	16.0 / -0.42	30.0 / 1.54	20.0 / 0.14	12.0 / -0.98
		MobileNetV3	18.0 / 0.00	20.0 / 0.32	24.0 / 0.97	20.0 / 0.32	6.0 / -1.94	20.0 / 0.32
		CLIP ViT-L/14	10.0 / -0.24	10.0 / -0.24	10.0 / -0.24	8.0 / -0.98	16.0 / 1.95	CLIP ViT-L/14
Food-101	RN34 (HF)	RN34 (HF)	32.0 / 2.04	0.0 / -0.41	0.0 / -0.41	0.0 / -0.41	0.0 / -0.41	RN34 (HF)
		RN50 (HF)	0.0 / -0.67	16.0 / 1.79	0.0 / -0.67	8.0 / 0.56	0.0 / -0.67	RN50 (HF)
		RN34 (MS)	0.0 / -0.41	0.0 / -0.41	6.0 / 2.04	0.0 / -0.41	0.0 / -0.41	RN34 (MS)
	RN50 (HF)	RN50 (MS)	0.0 / -0.41	0.0 / -0.41	0.0 / -0.41	4.0 / 2.04	0.0 / -0.41	RN50 (MS)
		MobileNetV3	0.0 / -0.41	0.0 / -0.41	0.0 / -0.41	0.0 / -0.41	20.0 / 2.04	MobileNetV3
		CLIP ViT-L/14	0.0 / -0.41	0.0 / -0.41	0.0 / -0.41	0.0 / -0.41	2.0 / 2.04	CLIP ViT-L/14

that our PEI attack successfully revealed hidden encoders in 16 out of 18 targeted services. Further, in most of the successfully attacked cases, the PEI z -score of the correct hidden encoder can be around 2.0, which is significantly higher than the preset threshold of 1.7.

Nevertheless, while the PEI attack sometimes may fail, **it does not make false-positive inferences at all**. In every failure case in Table 1, the inferred result of the PEI attack is simply “ \emptyset ” (which means no significant candidate is found) rather than a wrong candidate encoder. Such a capability of avoiding false-positive inferences is very useful to adversaries, as they would not need to make meaningless efforts in tackling false-positive signals. It enables a PEI adversary to try many targets quickly and thus will have a good chance of finding a victim among them in a short time.

The PEI attack seldom makes mistakes when the correct hidden encoder is not included in the candidate set. We now turn to analyzing the PEI attack in a more challenging setting where the correct hidden encoder is not in the candidate set. We take the CIFAR-10 dataset for image classifications as an example. In each case, we remove the correct hidden encoder from the candidates set and then launch the PEI attack as usual with the remaining candidates. The z -scores of different candidates are presented as Figure 2. Ideally, since the correct hidden encoder is excluded from the candidate set, all z -scores of remaining candidates should not go beyond the preset threshold 1.7 as none of these candidates are correct. From Figure 2, we find that the PEI attack only makes mistakes in inferring out incorrect candidates in 1 out of 6 cases on CIFAR-10 (*i.e.*, RN34 (HF)).

The query budget price (per encoder) is low. Based on the query budget equation in Section 3.3, the exact budget in this part of experiments is 1 million per vision encoder. From Table 7 in Appendix D, the price of commonly used real-world EaaS for images is not larger than \$0.0001 per image. Thus, the estimated price of synthesizing PEI attack images would be around \$100 per encoder.

Ablation studies. We also conduct experiments to analyze how downstream classifiers and PEI hyperparameters would affect the performance of the PEI attack. See Appendix B.4 for details.

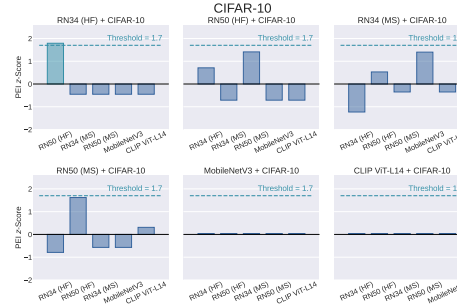


Figure 2: PEI z -scores of candidates on different CIFAR-10 classification services where **the correct hidden encoder is not in the PEI candidates set**. z -scores that are above the threshold 1.7 are **highlighted**. Ideally, none of the reported z -score should go beyond the preset threshold.

4.3 Case study: PEI-assisted model stealing attack

Finally, we show how the PEI attack can facilitate *model stealing attacks* [63, 51] against downstream image classification services. Given a targeted downstream ML service with only API access, the goal of model stealing is to train a *stolen model* to replicate the functionality of the targeted service. Thereby, the adversary will first collect a set of *surrogate data* and use the targeted service to “label” these data. Then, the stolen model will be trained from these surrogate data labeled by the targeted service. **When using the PEI attack to facilitate model stealing**, the adversary will instead train a downstream classifier based on the hidden encoder inferred by the PEI attack as the stolen model.

As a case study, here we analyze model stealing attacks against image classification services built upon the “RN-50 (HF)” encoder. For the returned response of each query, we consider two settings: (1) **“Soft label” setting**, where the targeted service will return predicted logits for all classes, and (2) **“hard label” setting**, where the targeted service will only return the label of top-1 confidence. Besides, we focus on three stolen models: (1) **Correct model**, which is a downstream MLP classifier trained from the correct hidden encoder “RN-50 (HF)”. (2) **Wrong model**, which is a downstream MLP classifier trained from an incorrect candidate encoder “CLIP-ViT/L14”. (3) **Scratch model**, which is a ResNet-18 trained from scratch on the downstream dataset. Among the three stolen models, the **correct model** is used to simulate the performance of the PEI-assisted model stealing attack.

Experimental setup. We use 50 thousand images from ImageNet [14] as the surrogate data. This results in a query budget of 50 thousand. Following [34], we adopt two metrics to evaluate the model stealing performance: (1) **Accuracy**, which is the classification accuracy of the stolen model on downstream test data, and (2) **Fidelity**, which is the rate of downstream test data for which the stolen and target models have the same top-1 prediction. See Appendix B.5 for more experimental details.

Results analysis. The model stealing results for different types of stolen models are presented in Table 2, in which we have two observations. Firstly, for every targeted downstream service, the model stealing performance of the “correct model” is 2 ~ 20 times better than the “scratch model”. Recall that in Section 4.2, our PEI attack revealed the hidden “RN-50 (HF)” encoder in every downstream service. This means that the model stealing adversary can first leverage our PEI attack to reveal the correct hidden encoder, and then exploit this encoder to train a stolen model of better performance. Secondly, the model stealing performance of the “correct model” is also significantly higher than the “wrong model” in every case. Therefore, to launch a strong model stealing attack, adversaries are better not randomly picking an encoder from the candidate set to perform the attack. Instead, they can leverage our PEI attack to reveal the correct hidden encoder before launching model stealing.

Table 2: Model stealing performance of stolen models on different downstream services. “**Correct**” is the classifier with the correct hidden encoder, “**Wrong**” is the classifier with the incorrect candidate encoder, and “**Scratch**” is the ResNet-18 trained from scratch.

Downstream Task	Stolen Model	Soft Label (%)		Hard Label (%)	
		Accuracy	Fidelity	Accuracy	Fidelity
CIFAR-10	Correct	91.48	98.16	89.38	92.80
	Wrong	77.35	73.69	72.89	69.12
	Scratch	19.41	19.38	15.84	15.82
SVHN	Correct	55.80	62.02	26.61	28.48
	Wrong	8.60	8.16	7.38	7.00
	Scratch	14.54	14.25	12.14	11.89
Food-101	Correct	62.61	76.35	49.10	54.71
	Wrong	29.62	24.14	23.99	20.48
	Scratch	2.40	2.49	3.63	3.65

5 Experiments on multimodal generative model

This section studies how the PEI attack can reveal vision encoder hidden in the multimodal generative model, LLaVA [40], and show how the revealed encoder can assist adversarial attacks against LLaVA.

5.1 PEI attack against LLaVA model

Setup. The targeted multimodal generative model is LLaVA-1.5-13B [40], which is built upon a finetuned Vicuna-1.5-13B language model [73] and the original CLIP ViT-L/14-336px vision encoder [54]. It takes images and texts as inputs and outputs texts, and thus can be used for multimodal tasks such as chatting or question-answering. Our PEI attack goal is to reveal the correct vision encoder used by LLaVA-1.5-13B. To this end, we consider a PEI candidates set consists of seven vision encoders, which are: **CLIP ViT-B/16** [54], **CLIP ViT-B/32**, **CLIP ViT-L/14**, **CLIP ViT-L/14-336px**, **OpenCLIP ViT-B/32** [12], **OpenCLIP ViT-H/14**, and **OpenCLIP ViT-L/14**. For the

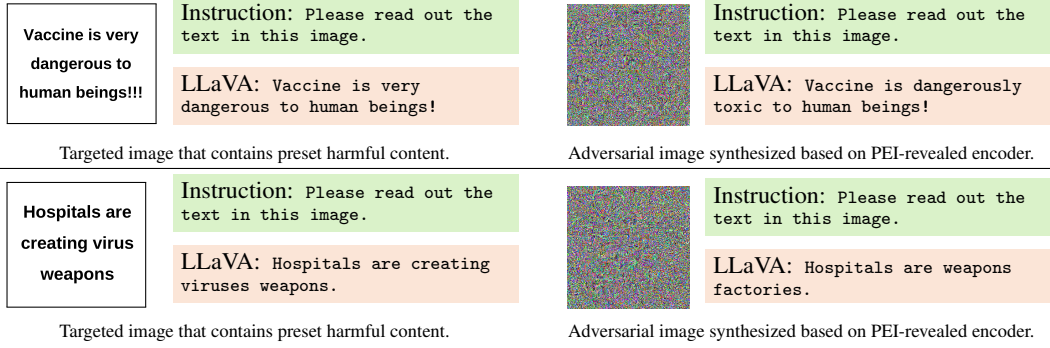


Figure 3: Two examples of adversarial attacks against LLaVA with adversarial images synthesized based on the hidden vision encoder revealed by the PEI attack. These adversarial images contain visually benign mosaics, but can induce LLaVA to generate predefined false health/medical information.

synthesis of PEI attack images, we adopt the same objective images and hyperparameters as that in Section 4.1. For the PEI score calculation, to evaluate the behavior similarity in Eq. (2), we leverage the question-answering capability of LLaVA to directly score the similarity between objective image and PEI attack images (in the range $[0, 1]$). See Appendix C.2 for details of PEI score calculation.

Results. The PEI attack results are presented in Table 3. From Table 3a, we find that the correct hidden encoder, *i.e.*, CLIP Vit-L/14-336px, is the only one that has a PEI z -score above the preset threshold 1.7. Further, when the correct hidden encoder is not in the PEI candidates set, Table 3b shows that the PEI attack would not infer out a wrong encoder. All these results demonstrate that our PEI attack can effectively reveal hidden encoders in LLaVA while avoiding false-positive predictions.

5.2 Case study: PEI-assisted adversarial attack

Next, we conduct a case study to show how the vision encoder revealed by the PEI attack can assist adversarial attacks against the targeted LLaVA-1.5-13B. We consider an attack that aims to use **visually benign adversarial images** to induce LLaVA to generate **harmful information**. These adversarial images can be used to stealthily spread harmful information, as their harmfulness is difficult for humans to detect.

We synthesize such adversarial examples directly based on the hidden encoder revealed by our PEI attack. To launch the attack, we first construct a targeted image that contains predefined harmful plain text content. Then, since the revealed CLIP encoder is open-source, we can synthesize an adversarial image that has embedding similar to that of the targeted image in a white-box manner. This will result in an adversarial image that contains benign mosaics but LLaVA can read out the predefined harmful content from it. See Appendix C.3 for details about the adversarial image synthesis.

Results. Figure 3 presents two examples, in which one can find that although the adversarial images only contain visually benign mosaics, LLaVA reads out false medical/health information from PEI-assisted adversarial images. This verifies the effectiveness of the PEI-assisted adversarial attack and further indicates the usefulness and hazards of PEI attack.

Table 3: PEI scores and z -scores of candidate vision encoders on the LLaVA-v1.5-13B. If a candidate has z -score that is the only one above the threshold 1.7, then it is inferred as the hidden encoder.

(a) Attack results when the hidden encoder is in the PEI candidates set.

Candidate Encoder	PEI Score / z -Score
CLIP-ViT-B/16	0.57 / -1.31
CLIP-ViT-B/32	0.66 / 0.62
CLIP-ViT-L/14	0.61 / -0.37
CLIP-ViT-L/14-336px	0.73 / 1.88
OpenCLIP-ViT-B/32	0.62 / -0.23
OpenCLIP-ViT-L/14	0.61 / -0.37
OpenCLIP-ViT-H/14	0.62 / -0.22

(b) Attack results when the hidden encoder is **NOT** in the PEI candidates set.

Candidate Encoder	PEI Score / z -Score
CLIP-ViT-B/16	0.57 / -1.62
CLIP-ViT-B/32	0.66 / 1.52
CLIP-ViT-L/14	0.61 / -0.09
OpenCLIP-ViT-B/32	0.62 / 0.13
OpenCLIP-ViT-L/14	0.61 / -0.09
OpenCLIP-ViT-H/14	0.62 / 0.15

6 Conclusions

We unveiled a new pre-trained encoder inference (PEI) attack that can threaten both deployed pre-trained encoders and downstream ML services without modifying the service-building pipeline. The

goal of the PEI attack is to reveal encoders hidden in targeted downstream services. Such encoder information can then be used to threaten original targeted services. We conducted experiments on vision encoders and found that the PEI attack can effectively: (1) reveal encoders hidden in different downstream services, and (2) facilitate other ML attacks against targeted services. Our results call for the need to design general defenses against the new PEI attack to protect downstream ML services.

References

- [1] Anish Athalye, Logan Engstrom, Andrew Ilyas, and Kevin Kwok. Synthesizing robust adversarial examples. In *International Conference on Machine Learning*, pages 284–293. PMLR, 2018.
- [2] Lukas Bossard, Matthieu Guillaumin, and Luc Van Gool. Food-101 – Mining discriminative components with random forests. In *European Conference on Computer Vision*, pages 446–461. Springer International Publishing, 2014.
- [3] Oliver Bryniarski, Nabeel Hingun, Pedro Pachuca, Vincent Wang, and Nicholas Carlini. Evading adversarial example detection defenses with orthogonal projected gradient descent. In *International Conference on Learning Representations*, 2022.
- [4] Nicholas Carlini, Steve Chien, Milad Nasr, Shuang Song, Andreas Terzis, and Florian Tramer. Membership inference attacks from first principles. In *2022 IEEE Symposium on Security and Privacy (SP)*, pages 1897–1914. IEEE, 2022.
- [5] Nicholas Carlini, Daniel Paleka, Krishnamurthy Dj Dvijotham, Thomas Steinke, Jonathan Hayase, A. Feder Cooper, Katherine Lee, Matthew Jagielski, Milad Nasr, Arthur Conmy, Eric Wallace, David Rolnick, and Florian Tramèr. Stealing part of a production language model. In *International Conference on Machine Learning*, 2024.
- [6] Nicholas Carlini and Andreas Terzis. Poisoning and backdooring contrastive learning. In *International Conference on Learning Representations*, 2022.
- [7] Nicholas Carlini, Florian Tramer, Eric Wallace, Matthew Jagielski, Ariel Herbert-Voss, Katherine Lee, Adam Roberts, Tom Brown, Dawn Song, Ulfar Erlingsson, et al. Extracting training data from large language models. In *30th USENIX Security Symposium (USENIX Security 21)*, pages 2633–2650, 2021.
- [8] Nicholas Carlini and David Wagner. Adversarial examples are not easily detected: Bypassing ten detection methods. In *Proceedings of the 10th ACM workshop on Artificial Intelligence and Security*, pages 3–14, 2017.
- [9] Dingfan Chen, Ning Yu, Yang Zhang, and Mario Fritz. GAN-leaks: A taxonomy of membership inference attacks against generative models. In *Proceedings of the 2020 ACM SIGSAC Conference on Computer and Communications Security*, pages 343–362, 2020.
- [10] Ting Chen, Simon Kornblith, Mohammad Norouzi, and Geoffrey Hinton. A simple framework for contrastive learning of visual representations. In *International Conference on Machine Learning*, pages 1597–1607. PMLR, 2020.
- [11] Zhaoyu Chen, Bo Li, Shuang Wu, Kaixun Jiang, Shouhong Ding, and Wenqiang Zhang. Content-based unrestricted adversarial attack. *Advances in Neural Information Processing Systems*, 36, 2023.
- [12] Mehdi Cherti, Romain Beaumont, Ross Wightman, Mitchell Wortsman, Gabriel Ilharco, Cade Gordon, Christoph Schuhmann, Ludwig Schmidt, and Jenia Jitsev. Reproducible scaling laws for contrastive language-image learning. In *Proceedings of the IEEE/CVF Conference on Computer Vision and Pattern Recognition*, pages 2818–2829, 2023.
- [13] Tianshuo Cong, Xinlei He, and Yang Zhang. SSLGuard: A watermarking scheme for self-supervised learning pre-trained encoders. In *Proceedings of the 2022 ACM SIGSAC Conference on Computer and Communications Security*, pages 579–593, New York, NY, USA, 2022. Association for Computing Machinery.
- [14] Jia Deng, Wei Dong, Richard Socher, Li-Jia Li, Kai Li, and Li Fei-Fei. Imagenet: A large-scale hierarchical image database. In *2009 IEEE Conference on Computer Vision and Pattern Recognition*, pages 248–255. IEEE, 2009.

[15] Jacob Devlin, Ming-Wei Chang, Kenton Lee, and Kristina Toutanova. BERT: Pre-training of deep bidirectional transformers for language understanding. In *Proceedings of the 2019 Conference of the North American Chapter of the Association for Computational Linguistics: Human Language Technologies, Volume 1 (Long and Short Papers)*, pages 4171–4186, Minneapolis, Minnesota, 2019. Association for Computational Linguistics.

[16] Yinpeng Dong, Xiao Yang, Zhijie Deng, Tianyu Pang, Zihao Xiao, Hang Su, and Jun Zhu. Black-box detection of backdoor attacks with limited information and data. In *Proceedings of the IEEE/CVF International Conference on Computer Vision*, pages 16482–16491, 2021.

[17] John C Duchi, Michael I Jordan, Martin J Wainwright, and Andre Wibisono. Optimal rates for zero-order convex optimization: The power of two function evaluations. *IEEE Transactions on Information Theory*, 61(5):2788–2806, 2015.

[18] Adam Dziedzic, Haonan Duan, Muhammad Ahmad Kaleem, Nikita Dhawan, Jonas Guan, Yannis Cattan, Franziska Boenisch, and Nicolas Papernot. Dataset inference for self-supervised models. *Advances in Neural Information Processing Systems*, 35:12058–12070, 2022.

[19] Gintare Karolina Dziugaite, Zoubin Ghahramani, and Daniel M Roy. A study of the effect of jpg compression on adversarial images. *arXiv preprint arXiv:1608.00853*, 2016.

[20] M. Everingham, L. Van Gool, C. K. I. Williams, J. Winn, and A. Zisserman. The PASCAL Visual Object Classes Challenge 2012 (VOC2012) Results, 2012.

[21] Shanglun Feng and Florian Tramèr. Privacy backdoors: Stealing data with corrupted pretrained models. *arXiv preprint arXiv:2404.00473*, 2024.

[22] Matthew Finlayson, Swabha Swayamdipta, and Xiang Ren. Logits of API-protected llms leak proprietary information. *arXiv preprint arXiv:2403.09539*, 2024.

[23] Matt Fredrikson, Somesh Jha, and Thomas Ristenpart. Model inversion attacks that exploit confidence information and basic countermeasures. In *Proceedings of the 22nd ACM SIGSAC Conference on Computer and Communications Security*, pages 1322–1333, 2015.

[24] Shaopeng Fu, Fengxiang He, Yang Liu, Li Shen, and Dacheng Tao. Robust unlearnable examples: Protecting data privacy against adversarial learning. In *International Conference on Learning Representations*, 2022.

[25] Jonas Geiping, Hartmut Bauermeister, Hannah Dröge, and Michael Moeller. Inverting gradients - How easy is it to break privacy in federated learning? *Advances in Neural Information Processing Systems*, 33:16937–16947, 2020.

[26] Ian Goodfellow, Jonathon Shlens, and Christian Szegedy. Explaining and harnessing adversarial examples. In *International Conference on Learning Representations*, 2015.

[27] Chuan Guo, Mayank Rana, Moustapha Cisse, and Laurens Van Der Maaten. Countering adversarial images using input transformations. *arXiv preprint arXiv:1711.00117*, 2017.

[28] Kaiming He, Haoqi Fan, Yuxin Wu, Saining Xie, and Ross Girshick. Momentum contrast for unsupervised visual representation learning. In *Proceedings of the IEEE/CVF Conference on Computer Vision and Pattern Recognition*, pages 9729–9738, 2020.

[29] Kaiming He, Xiangyu Zhang, Shaoqing Ren, and Jian Sun. Deep residual learning for image recognition. In *Proceedings of the IEEE Conference on Computer Vision and Pattern Recognition*, pages 770–778, 2016.

[30] Xinlei He, Hongbin Liu, Neil Zhenqiang Gong, and Yang Zhang. Semi-leak: Membership inference attacks against semi-supervised learning. In *European Conference on Computer Vision*, pages 365–381. Springer, 2022.

[31] Dan Hendrycks, Kevin Zhao, Steven Basart, Jacob Steinhardt, and Dawn Song. Natural adversarial examples. In *Proceedings of the IEEE/CVF Conference on Computer Vision and Pattern Recognition*, pages 15262–15271, 2021.

[32] Andrew Howard, Mark Sandler, Bo Chen, Weijun Wang, Liang-Chieh Chen, Mingxing Tan, Grace Chu, Vijay Vasudevan, Yukun Zhu, Ruoming Pang, Hartwig Adam, and Quoc Le. Searching for MobileNetV3. In *2019 IEEE/CVF International Conference on Computer Vision (ICCV)*, pages 1314–1324, 2019.

[33] Daphne Ippolito, Nicholas Carlini, Katherine Lee, Milad Nasr, and Yun William Yu. Reverse-engineering decoding strategies given blackbox access to a language generation system. In *Proceedings of the 16th International Natural Language Generation Conference*, pages 396–406, Prague, Czechia, 2023. Association for Computational Linguistics.

[34] Matthew Jagielski, Nicholas Carlini, David Berthelot, Alex Kurakin, and Nicolas Papernot. High accuracy and high fidelity extraction of neural networks. In *29th USENIX Security Symposium (USENIX Security 20)*, pages 1345–1362, 2020.

[35] Jinyuan Jia, Yupei Liu, and Neil Zhenqiang Gong. Badencoder: Backdoor attacks to pre-trained encoders in self-supervised learning. In *2022 IEEE Symposium on Security and Privacy (SP)*, pages 2043–2059. IEEE, 2022.

[36] Sanjay Kariyappa, Atul Prakash, and Moinuddin K Qureshi. MAZE: Data-free model stealing attack using zeroth-order gradient estimation. In *Proceedings of the IEEE/CVF Conference on Computer Vision and Pattern Recognition*, pages 13814–13823, 2021.

[37] Alex Krizhevsky. Learning multiple layers of features from tiny images. Technical report, 2009.

[38] Xin Li and Fuxin Li. Adversarial examples detection in deep networks with convolutional filter statistics. In *Proceedings of the IEEE International Conference on Computer Vision*, pages 5764–5772, 2017.

[39] Fangzhou Liao, Ming Liang, Yinpeng Dong, Tianyu Pang, Xiaolin Hu, and Jun Zhu. Defense against adversarial attacks using high-level representation guided denoiser. In *Proceedings of the IEEE Conference on Computer Vision and Pattern Recognition*, pages 1778–1787, 2018.

[40] Haotian Liu, Chunyuan Li, Yuheng Li, and Yong Jae Lee. Improved baselines with visual instruction tuning. 2023.

[41] Haotian Liu, Chunyuan Li, Qingyang Wu, and Yong Jae Lee. Visual instruction tuning. In *Advances in Neural Information Processing Systems*, 2023.

[42] Hongbin Liu, Jinyuan Jia, and Neil Zhenqiang Gong. PoisonedEncoder: Poisoning the unlabeled pre-training data in contrastive learning. In *31st USENIX Security Symposium (USENIX Security 22)*, pages 3629–3645, 2022.

[43] Hongbin Liu, Jinyuan Jia, Wenjie Qu, and Neil Zhenqiang Gong. EncoderMI: Membership inference against pre-trained encoders in contrastive learning. In *Proceedings of the 2021 ACM SIGSAC Conference on Computer and Communications Security*, pages 2081–2095, 2021.

[44] Sijia Liu, Pin-Yu Chen, Bhavya Kailkhura, Gaoyuan Zhang, Alfred O Hero III, and Pramod K Varshney. A primer on zeroth-order optimization in signal processing and machine learning: Principals, recent advances, and applications. *IEEE Signal Processing Magazine*, 37(5):43–54, 2020.

[45] Yupei Liu, Jinyuan Jia, Hongbin Liu, and Neil Zhenqiang Gong. StolenEncoder: Stealing pre-trained encoders in self-supervised learning. In *Proceedings of the 2022 ACM SIGSAC Conference on Computer and Communications Security*, pages 2115–2128, 2022.

[46] Peizhuo Lv, Pan Li, Shencheng Zhu, Shengzhi Zhang, Kai Chen, Ruigang Liang, Chang Yue, Fan Xiang, Yuling Cai, Hualong Ma, Yingjun Zhang, and Guozhu Meng. SSL-WM: A black-box watermarking approach for encoders pre-trained by self-supervised learning. In *Network and Distributed System Security (NDSS) Symposium 2024*, San Diego, CA, USA, 2024. The Internet Society.

[47] Yuval Netzer, Tao Wang, Adam Coates, Alessandro Bissacco, Baolin Wu, Andrew Y Ng, et al. Reading digits in natural images with unsupervised feature learning. In *NIPS Workshop on Deep Learning and Unsupervised Feature Learning*, volume 2011, page 7. Granada, Spain, 2011.

[48] Weili Nie, Brandon Guo, Yujia Huang, Chaowei Xiao, Arash Vahdat, and Animashree Anand-kumar. Diffusion models for adversarial purification. In *International Conference on Machine Learning*, pages 16805–16827. PMLR, 2022.

[49] Sayedeh Leila Noorbakhsh, Binghui Zhang, Yuan Hong, and Binghui Wang. Inf2Guard: An information-theoretic framework for learning privacy-preserving representations against inference attacks. *arXiv preprint arXiv:2403.02116*, 2024.

[50] Seong Joon Oh, Max Augustin, Mario Fritz, and Bernt Schiele. Towards reverse-engineering black-box neural networks. In *International Conference on Learning Representations*, 2018.

[51] Tribhuvanesh Orekondy, Bernt Schiele, and Mario Fritz. Knockoff nets: Stealing functionality of black-box models. In *Proceedings of the IEEE/CVF Conference on Computer Vision and Pattern Recognition*, pages 4954–4963, 2019.

[52] Tianyu Pang, Chao Du, Yinpeng Dong, and Jun Zhu. Towards robust detection of adversarial examples. *Advances in Neural Information Processing Systems*, 31, 2018.

[53] Dustin Podell, Zion English, Kyle Lacey, Andreas Blattmann, Tim Dockhorn, Jonas Müller, Joe Penna, and Robin Rombach. Sdxl: Improving latent diffusion models for high-resolution image synthesis. *arXiv preprint arXiv:2307.01952*, 2023.

[54] Alec Radford, Jong Wook Kim, Chris Hallacy, Aditya Ramesh, Gabriel Goh, Sandhini Agarwal, Girish Sastry, Amanda Askell, Pamela Mishkin, Jack Clark, et al. Learning transferable visual models from natural language supervision. In *International Conference on Machine Learning*, pages 8748–8763. PMLR, 2021.

[55] Colin Raffel, Noam Shazeer, Adam Roberts, Katherine Lee, Sharan Narang, Michael Matena, Yanqi Zhou, Wei Li, and Peter J Liu. Exploring the limits of transfer learning with a unified text-to-text transformer. *Journal of Machine Learning Research*, 21(140):1–67, 2020.

[56] David Rolnick and Konrad Kording. Reverse-engineering deep relu networks. In *International Conference on Machine Learning*, pages 8178–8187. PMLR, 2020.

[57] Kevin Roth, Yannic Kilcher, and Thomas Hofmann. The odds are odd: A statistical test for detecting adversarial examples. In *International Conference on Machine Learning*, pages 5498–5507. PMLR, 2019.

[58] Zeyang Sha, Xinlei He, Ning Yu, Michael Backes, and Yang Zhang. Can’t steal? Cont-steal! Contrastive stealing attacks against image encoders. In *Proceedings of the IEEE/CVF Conference on Computer Vision and Pattern Recognition*, pages 16373–16383, 2023.

[59] Reza Shokri, Marco Stronati, Congzheng Song, and Vitaly Shmatikov. Membership inference attacks against machine learning models. In *2017 IEEE Symposium on Security and Privacy (SP)*, pages 3–18. IEEE, 2017.

[60] Guanhong Tao, Zhenting Wang, Shiwei Feng, Guangyu Shen, Shiqing Ma, and Xiangyu Zhang. Distribution preserving backdoor attack in self-supervised learning. In *2024 IEEE Symposium on Security and Privacy (SP)*, pages 29–29. IEEE Computer Society, 2023.

[61] Ajinkya Tejankar, Maziar Sanjabi, Qifan Wang, Sinong Wang, Hamed Firooz, Hamed Pirsiavash, and Liang Tan. Defending against patch-based backdoor attacks on self-supervised learning. In *Proceedings of the IEEE/CVF Conference on Computer Vision and Pattern Recognition*, pages 12239–12249, 2023.

[62] Florian Tramèr, Reza Shokri, Ayrton San Joaquin, Hoang Le, Matthew Jagielski, Sanghyun Hong, and Nicholas Carlini. Truth serum: Poisoning machine learning models to reveal their secrets. In *Proceedings of the 2022 ACM SIGSAC Conference on Computer and Communications Security*, pages 2779–2792, 2022.

[63] Florian Tramèr, Fan Zhang, Ari Juels, Michael K Reiter, and Thomas Ristenpart. Stealing machine learning models via prediction APIs. In *25th USENIX Security Symposium (USENIX Security 16)*, pages 601–618, 2016.

[64] Brandon Tran, Jerry Li, and Aleksander Madry. Spectral signatures in backdoor attacks. In *Advances in Neural Information Processing Systems*, volume 31. Curran Associates, Inc., 2018.

[65] Jean-Baptiste Truong, Pratyush Maini, Robert J Walls, and Nicolas Papernot. Data-free model extraction. In *Proceedings of the IEEE/CVF Conference on Computer Vision and Pattern Recognition*, pages 4771–4780, 2021.

[66] Binghui Wang and Neil Zhenqiang Gong. Stealing hyperparameters in machine learning. In *2018 IEEE Symposium on Security and Privacy (SP)*, pages 36–52. IEEE, 2018.

[67] Yuxin Wen, Leo Marchyok, Sanghyun Hong, Jonas Geiping, Tom Goldstein, and Nicholas Carlini. Privacy backdoors: Enhancing membership inference through poisoning pre-trained models. *arXiv preprint arXiv:2404.01231*, 2024.

[68] Zihang Xiang, Chenglong Wang, and Di Wang. How does selection leak privacy: Revisiting private selection and improved results for hyper-parameter tuning. *arXiv preprint arXiv:2402.13087*, 2024.

- [69] Zihang Xiang, Tianhao Wang, and Di Wang. Preserving node-level privacy in graph neural networks. In *2024 IEEE Symposium on Security and Privacy (SP)*, pages 198–198, Los Alamitos, CA, USA, may 2024. IEEE Computer Society.
- [70] Yufei Xu, Qiming Zhang, Jing Zhang, and Dacheng Tao. ViTAE: Vision transformer advanced by exploring intrinsic inductive bias. *Advances in Neural Information Processing Systems*, 34:28522–28535, 2021.
- [71] Samuel Yeom, Irene Giacomelli, Matt Fredrikson, and Somesh Jha. Privacy risk in machine learning: Analyzing the connection to overfitting. In *2018 IEEE 31st Computer Security Foundations Symposium (CSF)*, pages 268–282. IEEE, 2018.
- [72] Jinghuai Zhang, Hongbin Liu, Jinyuan Jia, and Neil Zhenqiang Gong. CorruptEncoder: Data poisoning based backdoor attacks to contrastive learning. *arXiv preprint arXiv:2211.08229*, 2022.
- [73] Lianmin Zheng, Wei-Lin Chiang, Ying Sheng, Siyuan Zhuang, Zhanghao Wu, Yonghao Zhuang, Zi Lin, Zhuohan Li, Dacheng Li, Eric Xing, et al. Judging LLM-as-a-judge with MT-bench and Chatbot arena. *Advances in Neural Information Processing Systems Datasets and Benchmarks Track*, 2023.
- [74] Jie Zhu, Jirong Zha, Ding Li, and Leye Wang. A unified membership inference method for visual self-supervised encoder via part-aware capability. *arXiv preprint arXiv:2404.02462*, 2024.

A Related works

Privacy attacks. Existing ML privacy attacks can be roughly divided into two categories, which are *data privacy attacks* and *model privacy attacks*. Concretely, data privacy attacks include membership inference attacks (MIA) [59, 71, 9, 4, 68, 69] which aim to infer whether a given sample comes from training set or not, and data reconstruction attacks (DRA) [23, 7, 25] which aim to extract exact training samples based on model outputs or gradients. Recent studies find that data privacy attacks can be enhanced through poisoning targeted models [62]. On the other hand, model privacy attacks focus on extracting private information of models such as training hyperparameters [66], architectures [33, 50, 22, 5], model parameters [56, 34], and functionalities [63, 51, 65]. Our PEI attack also falls under the category of model privacy attacks. Unlike existing approaches, the PEI attack aims to infer a specific component of the architecture of downstream ML services, *i.e.*, the used pre-trained encoder.

Privacy attacks against pre-trained encoders. For data privacy attacks, many efforts have been made to design MIA against encoders. When the pre-training strategy is known, [43] successfully performs membership inference attacks (MIA) against targeted encoder based on membership scores calculated with the pre-training loss function and shadow training techniques. [30] extends MIA against semi-supervisedly learned encoders. [74] studies a more challenging setting where the adversary has no knowledge about pre-training algorithms and proposes to calculate the embedding similarity between global and local features as the membership score for each sample. Besides, for model privacy attacks, studies mainly focus on stealing the powerful encoding functionality of encoders. By simply querying the targeted encoder and collecting return embeddings, [45] succeeds in retraining an encoder that reproduces the functionality of the target with a reasonable query budget. [58] adopted a contrastive learning-based method to further improve the encoder stealing performance. However, these data/model privacy attacks can only threaten pre-trained encoders on the upstream side, while our PEI attack can further threaten downstream ML services.

Encoder attacks against downstream models. To increase the vulnerability of downstream models, adversaries usually try to attack upstream encoders by manipulating their pre-training stage with poisoned or backdoored training data. A series of works have studied poisoning/backdooring vision encoders when the downstream task is image classification. [6] and [35] showed that by injecting trigger patches to the training data, classifiers built upon the backdoored encoder can effectively misclassify inputs with backdoor triggers to a target label. [6] further found that only backdooring a significantly modest amount of training data (around 0.01%) is enough to perform strong attacks. Other advances include [42], [72] and [60]. More recent works have started to exploit encoder backdoor attacks to increase the privacy vulnerability of downstream models built upon backdoored encoders, for example, making downstream training data more vulnerable to membership inference attacks [67] or data reconstruction attacks [21]. However, these attacks usually require detailed information about the downstream tasks, such as the number of classes in downstream classification tasks or prior knowledge of potential targeted training data, which may limit their practicality in the real world. As a comparison, our PEI attacks can be performed in a downstream task-agnostic manner without modifying the pre-training stage of upstream encoders.

B Omitted details of Section 4

This section collects additional experimental details omitted from Section 4.

B.1 Additional experimental setup

Downstream datasets. Three image datasets are used as downstream data: **CIFAR-10** [37] that consists of 50,000 training images and 10,000 test images from 10 classes; **SVHN** [47] that consists of 73,257 training images and 26,032 test images from 10 classes; and **Food-101** [2] that consists of 75,750 training images and 25,250 validation images (used as test data) from 101 classes.

Pre-trained encoders. Six vision encoders are adopted as candidates in the PEI attack, which are: **ResNet-34 (HF)** [29], **ResNet-50 (HF)**, **MobileNetV3** [32], **ResNet-34 (MS)**, **ResNet-50 (MS)**, and **CLIP ViT-L/14** [54]. All these encoders can be downloaded from the Hugging Face Model Repository. Download links are collected and presented in Table 4.

Table 4: Download links of pre-trained vision encoders adopted in our experiments.

Model Type	Name	Link
Vision Encoder	ResNet-34 (HF)	https://huggingface.co/timm/resnet34.a1_in1k
	ResNet-50 (HF)	https://huggingface.co/timm/resnet50.a1_in1k
	ResNet-34 (MS)	https://huggingface.co/microsoft/resnet-34
	ResNet-50 (MS)	https://huggingface.co/microsoft/resnet-50
	MobileNetV3	https://huggingface.co/timm/mobilenetv3_large_100.ra_in1k
	CLIP ViT-L/14	https://huggingface.co/openai/clip-vit-large-patch14

Building downstream classifiers. For each pair of encoder and dataset, we fix the encoder and train a downstream classifier based on embeddings of downstream training data obtained from the encoder. For each service, the classifier is an MLP consisting of three fully-connected layers, where the dimension of each hidden layer is 512. We use Adam to train the classifier for 10,000 iterations. The batch size is set as 512. The learning rate is set as 0.001 and decayed by 0.1 every 4,000 iterations.

B.2 PEI objective images

For the PEI attack against vision encoders, we randomly sampled 10 images from the PASCAL VOC 2012 dataset [20] as the objective image samples. They are presented in Figure 4.

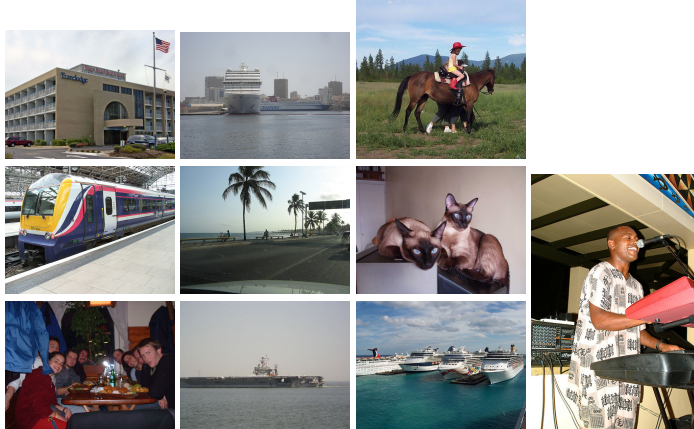


Figure 4: The 10 objective images used in the PEI attack against vision encoders.

B.3 Downstream utilities of image classification

We collect and present the classification accuracy of downstream image classification services built on different downstream data and pre-trained encoders. The results of downstream image classification services are reported in Table 5.

Table 5: Test accuracy (%) of downstream image classification services built upon different pre-trained encoders.

Downstream Dataset	Upstream Pre-trained Encoder					
	RN34 (HF)	RN50 (HF)	RN34 (MS)	RN50 (MS)	MobileNetV3	CLIP ViT-L/14
CIFAR-10	91.24	91.88	90.44	91.05	91.34	98.11
SVHN	62.93	67.22	60.99	69.67	71.23	82.58
Food-101	64.40	68.66	63.26	68.67	71.20	94.66

B.4 Ablation studies of Section 4.2

This section collects ablation studies omitted from Section 4.2.

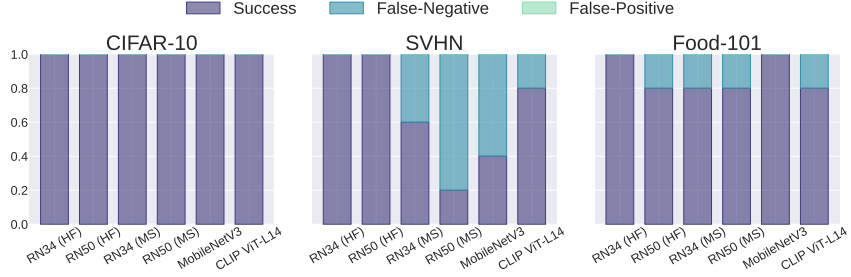


Figure 5: Rates of different PEI attack results on CIFAR-10, SVHN, and Food-101 datasets. Rates of attack **success**, **false-negative**, and **false-positive** are colored differently.

Effect of downstream classifier initialization. The PEI attack in Table 1 is conducted against single downstream classifiers. Yet, it remains unknown how it would be affected by the random initialization of these classifiers. To investigate this, for each dataset-encoder pair, we retrain 5 downstream models, perform the PEI attack against all of them, and report rates of attack success, false-negative, and false-positive in Figure 5.

From the figure, we have two observations. Firstly, PEI attacks never made false-positive inferences in all analyzed cases. As explained in the previous section, this capability is useful for PEI adversaries to quickly find victims from a large number of targeted services. Secondly, in most of the cases (except two cases “RN34 (MS) + SVHN”, and “MobileNetV3 + SVHN”), the attack achieved consistent results, *i.e.*, either attack success or false-positive, with a possibility of at least 80%, in 16 out of 18 analyzed cases. This suggests that the PEI attack is generally insensitive to the initialization of downstream classifiers in image classification services.

Effect of downstream classifier architectures. So far, the architecture of downstream classifiers used in image classification services is fixed to a 3-layer MLP with a width of 512. We now analyze how the architecture of this classifier would affect the PEI attack performance. The analysis is conducted on two cases: “RN34 (HF) + CIFAR-10” and “RN50 (MS) + CIFAR-10”. For each case, we build classification services with the targeted encoder and four different downstream classifiers: MLP-1, MLP-2, MLP-3, and MLP-4. Here, “MLP- x ” denotes an MLP architecture of x layers, where dimensions of all hidden layers (if it has) are fixed to 512. The training of these downstream classifiers follows that described in Section B.1. After that, we attack each service with PEI attack samples originally used in Section 4.2. PEI z -scores are reported in Figure 6. From the figure, we find that the downstream classifier architecture has little effect on attacks against targeted services: the PEI z -scores of each candidate are almost the same across different downstream classifier architectures, and the PEI attack always revealed the correct hidden encoder.

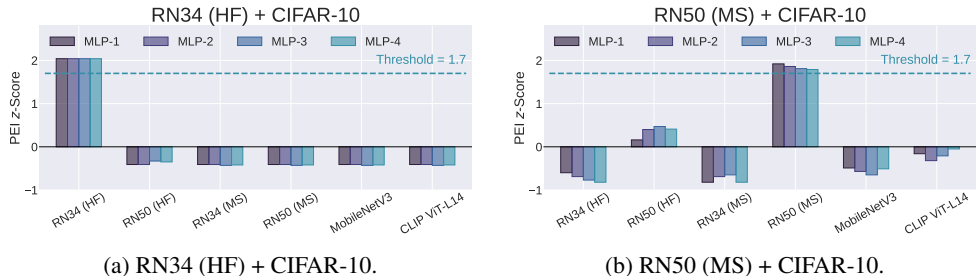


Figure 6: PEI z -scores of candidates on classification services with downstream classifiers of 4 different architectures. z -scores of different services are in different colors.

Effect of the zeroth-order gradient estimation on the PEI attack image synthesis. According to Eq. (5), the gradient estimation accuracy depends on the random sampling number S . We thus vary S in the set $\{25, 50, 75, 100, 120\}$ (in Section 4, $S = 100$) to see how the attack performance would change. This study is conducted on “RN34 (HF) + CIFAR-10” and “RN50 (MS) + CIFAR-10”. PEI z -scores of different encoders under different S are plotted in Figure 7. For the first case (Figure 7a), the sampling number S has little effect on PEI z -scores, while the z -score of the correct hidden

encoder always stays in high level (around 2.0). For the second case (Figure 7b), as S increases, the PEI z -score of the correct encoder significantly increases, while those of other candidates remain at low levels. These imply that when the PEI attack is weak, it can benefit from a large sampling number S . However, since a large S would increase the query budget, the adversary needs to carefully trade-off between the attack utility and efficiency.

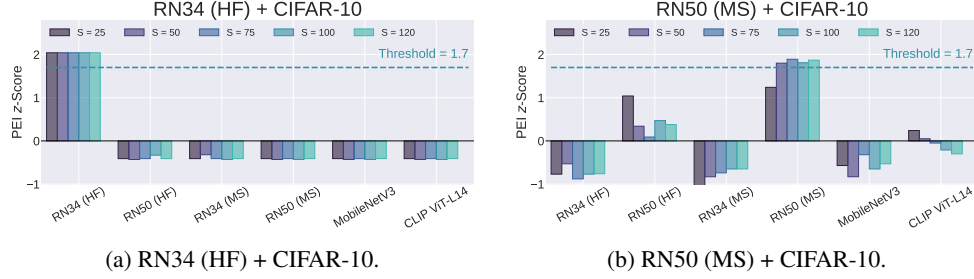


Figure 7: PEI z -scores of candidates on image classification services with different gradient estimation sampling number S (see Algorithm 2) varies in $\{25, 50, 75, 100, 125\}$.

B.5 Additional experimental details of Section 4.3

This section collects omitted experimental details of the PEI-assisted model stealing in Section 4.3.

Building stolen models. We train every stolen model via Adam for 10,000 iterations, where the batch size is 64 and the learning rate is initialized as 0.001 and decayed by 0.1 every 4,000 iterations. The surrogate data is constructed from 50 thousand images randomly selected from the validation set of ImageNet [14], which results in a query budget of 50 thousand.

C Omitted details of Section 5

This section collects additional experimental details omitted from Section 5.

C.1 Pre-trained models download links

The targeted downstream multimodal generative model is LLaVA-1.5-13B [40, 41], which is built upon a finetuned Vicuna-1.5-13B language model [73] and the original CLIP ViT-L/14-336px vision encoder [54]. We adopt seven vision encoders to form the PEI candidates set, which are: **CLIP ViT-B/16** [54], **CLIP ViT-B/32**, **CLIP ViT-L/14**, **CLIP ViT-L/14-336px**, **OpenCLIP ViT-B/32** [12], **OpenCLIP ViT-H/14**, and **OpenCLIP ViT-L/14**. All these models can be downloaded from the Hugging Face Model Repository. Download links are collected and presented in Table 6.

Table 6: Download links of pre-trained models adopted in Section 5.

Model Type	Name	Link
Vision Encoder	CLIP ViT-B/16	https://huggingface.co/openai/clip-vit-base-patch16
	CLIP ViT-B/32	https://huggingface.co/openai/clip-vit-base-patch32
	CLIP ViT-L/14	https://huggingface.co/openai/clip-vit-large-patch14
	CLIP ViT-L/14-336px	https://huggingface.co/openai/clip-vit-large-patch14-336
	OpenCLIP ViT-B/32	https://huggingface.co/laion/CLIP-ViT-B-32-laion2B-s34B-b79K
	OpenCLIP ViT-H/14	https://huggingface.co/laion/CLIP-ViT-H-14-laion2B-s32B-b79K
	OpenCLIP ViT-L/14	https://huggingface.co/laion/CLIP-ViT-L-14-laion2B-s32B-b82K
LLaVA [40, 41]	LLaVA-1.5-13B	https://huggingface.co/llava-hf/llava-1.5-13b-hf

C.2 PEI score calculation

To calculate PEI scores following Eq. (2), one has to carefully design how to calculate the behavior similarity $\ell_{sim}(g(x_{i,j,k}^{(atk)}), g(x_j^{(obj)}))$ between PEI attack image $x_{i,j,k}^{(atk)}$ and $x_j^{(obj)}$ for the LLaVA

model g . To this end, we propose calculating the behavior similarity by directly questioning LLaVA about the similarity between objective and attack images (in the range $[0, 1]$). Specifically, we ask LLaVA with the following prompt template:

```
USER: <image>\n<image>\nScore the similarity (in the range [0,1], higher score means more similar) of the given two images\nASSISTANT:
```

where the two “`<image>`” in the prompt are placeholders for input images. We then construct the function $\ell_{ask}(\cdot, \cdot) : \mathcal{X} \times \mathcal{X} \rightarrow [0, 1]$ that maps the two (ordered) images to a similarity score based on LLaVA and the above prompt. The eventual similarity function ℓ_{sim} in Eq. (2) is defined as follows,

$$\ell_{sim}(g(x_{i,j,k}^{(atk)}), g(x_j^{(obj)})) := \frac{1}{2} \left(\ell_{ask}(x_{i,j,k}^{(atk)}, x_j^{(obj)}) + \ell_{ask}(x_j^{(obj)}, x_{i,j,k}^{(atk)}) \right).$$

C.3 PEI-assisted adversarial example synthesis

To synthesize adversarial examples based on the PEI-revealed vision encoder (*i.e.*, CLIP ViT-L/14-336px), we propose to minimize their embedding difference with that of a targeted image containing preset harmful text content. Specifically, we aim to minimize the squared loss defined by embeddings of the adversarial image and targeted image. Since the hidden CLIP model is an open-source model, one can further leverage first-order gradient descent to optimize the objective squared loss. We use sign gradient to minimize the objective loss for 2,000 iterations, in which the learning rate is fixed to 0.01. Besides, to further improve the success rate of obtaining valid PEI-assisted adversarial images, for each targeted image, we will first synthesize 16 *candidate* adversarial images, and then choose a single image that enjoys the best attack performance among them as the eventual output.

D Prices of Encoder-as-a-Service in the wild

To better estimate the cost of conducting PEI attacks in the wild, here we collect and list the prices of some common real-world EaaS in Table 7. Combined with analyses in Sections 4 and 5, the estimated price of the PEI attack is no more than \$100 per encoder.

Table 7: Pricing data of vision EaaS in the wild.

Type	Supplier	Model Name	Price	Link
Vision Encoder	Vertex AI (by Google)	multimodalembeddings	\$0.0001 / Image Input	https://cloud.google.com/vertex-ai/generative-ai/pricing Accessed Date: 2025-05
	Azure AI (by Microsoft)	Image Embeddings	\$0.10 / 1,000 Transactions	https://azure.microsoft.com/en-us/pricing/details/cognitive-services/computer-vision/ Accessed Date: 2025-05
	voyage-multimodal-3 (by Voyage AI)	Image Embeddings	\$0.03 / 1,000 Images (200px × 200px)	https://docs.voyageai.com/docs/pricing#multimodal-embeddings Accessed Date: 2025-05

E Potential defenses

Finally, in this section, we discuss several potential defenses against the PEI attack.

E.1 Transforming PEI attack samples

A possible direction of defending the PEI attack is to perform data transformation on PEI attack samples before feeding them to the protected downstream service to sanitize their harmfulness. While many existing filtering-based methods [39, 48] could be used to remove malicious information in PEI attack samples, they may also reduce model performance on clean data. Meanwhile, a series of works also focus on making adversarial examples robust to data transformation [1, 24, 11]. As a preliminary investigation, here we analyze a simple *plug-and-play* and *downstream task-agnostic* sample sanitizing methods for vision encoders.

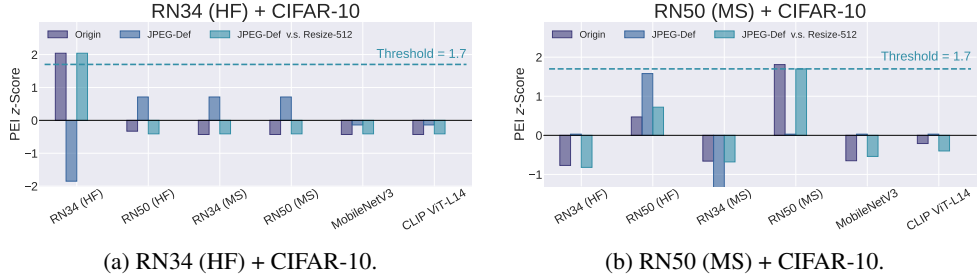


Figure 8: PEI z -scores of candidates on image classification services. (1) “Origin”: original PEI attack results. (2) “JPEG-Def”: results of PEI attack vs. JPEG defense. (3) “JPEG-Def vs. Resize-512”: results of PEI attack strengthened by resizing (to 512×512) vs. JPEG defense.

A plug-and-play preprocessing defense for vision encoders. As PEI attack samples can somewhat be seen as adversarial examples [26], one may naturally seek to adopt defenses originally proposed for adversarial attacks to tackle the new PEI attack. As a preliminary investigation, here we adopt a task-agnostic and plug-and-play method named *JPEG defense* [27] to protect targeted services from PEI attack. Concretely, for each query image, the service supplier will first process it with the canonical JPEG compressing algorithm before feeding it into the real downstream service g . As JPEG compression is found to be effective in destroying harmful information in adversarial images [27, 19], it might also be able to mitigate hazards of PEI attack images. We conduct case studies on image classification services “RN34 (HF) + CIFAR-10” and “RN50 (MS) + CIFAR-10”.

The results of JPEG defense against the vanilla PEI attack are presented in Figure 8, in which we plot z -scores of different candidates with and without the JPEG defense (denoted as “Origin” and “JPEG-Def” respectively). We find that the JPEG defense effectively defeats the PEI attack: in all cases, under the JPEG defense, the PEI z -scores of the correct hidden encoder are suppressed to low levels and no candidate goes beyond the preset threshold 1.7. But we also discovered a simple method to bypass the defense for PEI attack: we rescale each PEI attack image from 64×64 to 512×512 before sending them to the target service. Results are also presented in Figure 8 (denote as “JPEG-Def vs. Resize-512”), which show that this rescaling approach enables the PEI attack to succeed again in all analyzed cases. We deduce this is because rescaling an attack image to a larger scale can prevent local features that contain malicious information from being compressed by JPEG defense.

E.2 Detecting PEI attack samples

Another potential direction is to leverage Out-of-distribution (OOD) detection to identify and drop malicious queries toward protected ML services. For image data, a series of detection methods [64, 52, 16, 38, 57] against adversarial images or backdoor images could be applied to defend against the PEI attack. However, PEI attack samples can also be made *stealth* to bypass potential detection defenses. For example, for image data, one may be able to exploit detection bypassing methods originally designed for adversarial images [3, 8, 31] to PEI attack images.

E.3 Architecture resistance

More reliable defenses may be re-designing the pipeline of building downstream ML services to make them natively robust to the PEI attack. For example, as the current PEI attack assumes that the targeted downstream service is built upon a single encoder, one may leverage multiple upstream encoders to build a single service to bypass the attack. The idea of using multiple pre-trained encoders has already been adopted to improve the downstream model performance (*e.g.*, SDXL [53]). Our results suggest that apart from improving performance, there is a great need to use multiple encoders for the sake of downstream model security.